Temperature-dependent properties of CoFeB/MgO thin films: Experiments versus simulations

H. Sato,[1,2,3,4,*] P. Chureemart,[5,6] F. Matsukura,[1,2,3,4,7] R. W. Chantrell,[5] H. Ohno,[1,2,3,4,7] and R. F. L. Evans[5,†]

[1]*Center for Spintronics Research Network, Tohoku University, 2-1-1 Katahira, Aoba-ku, Sendai 980-8577, Japan*

[2]*Laboratory for Nanoelectronics and Spintronics, Research Institute of Electrical Communication, Tohoku University, 2-1-1 Katahira, Aoba-ku, Sendai 980-8577, Japan*

[3]*Center for Spintronics Integrated Systems, 2-1-1 Katahira, Aoba-ku, Tohoku University, Sendai 980-8577, Japan*

[4]*Center for Innovative Integrated Electronic Systems, Tohoku University, 468-1 Aramaki Aza Aoba, Aoba-ku, Sendai 980-0845, Japan*

[5]*Department of Physics, The University of York, York YO10 5DD, United Kingdom*

[6]*Department of Physics, Mahasarakham University, Mahasarakham 44150, Thailand*

[7]*WPI-Advanced Institute for Materials Research, Tohoku University, 2-1-1 Katahira, Aoba-ku, Sendai 980-8577, Japan*

(Received 17 October 2017; revised manuscript received 1 July 2018; published 14 December 2018)

CoFeB/MgO heterostructures are a promising candidate for an integral component of spintronic devices due to their high magnetic anisotropy, low Gilbert damping, and excellent magnetoresistive properties. Here, we present experimental measurements and atomistic simulations of the temperature and CoFeB thickness dependence of spontaneous magnetization and magnetic anisotropy in CoFeB/MgO ultrathin films. We find that the thermal fluctuations are different between the bulk and interface magnetizations, and that the interfacial anisotropy originates from a two-site anisotropic exchange interaction. These effects lead to a complex temperature and thickness dependence of the magnetic properties critical to device operation and stability at elevated temperatures.

DOI: 10.1103/PhysRevB.98.214428

I. INTRODUCTION

In recent years, an interfacial anisotropy at ferromagnetic metal (FM)/oxides has been an interesting subject in the field of spintronics because of its importance for applications. For instance, the interfacial anisotropy reduces the intrinsic critical current for spin-transfer-torque (STT)-induced magnetization switching in magnetic tunnel junctions (MTJs) with an in-plane easy axis (i-MTJs) without reduction of the thermal stability factor. In addition, the interfacial anisotropy enables the manufacture of MTJs with a perpendicular easy axis (p-MTJs) by reducing the FM layer thickness, which allows a higher efficiency for the STT switching compared to i-MTJs.

A large interfacial perpendicular anisotropy energy density K_i of $1.18\,\mathrm{mJ/m^2}$ at a FM/oxide interface was reported in a single-crystal Fe substrate/MgO/Fe/Au structure [1]. The presence of the interfacial anisotropy at FM/oxide interfaces was also reported in polycrystalline films with Pt/Co(Fe)/MO_x (M: Al, Mg, Ta, or Ru) [2,3] and MgO/CoFeB/Pt structures [4]. In Ta/CoFeB/MgO structure, a technologically relevant structure owing to its high tunnel magnetoresistance ratio [5,6], the presence of K_i was also found [7]. This brought about the demonstration of high-performance p-MTJs with Ta/CoFeB/MgO at a junction diameter of 40 nm [8], which triggered ongoing intensive studies on p-MTJs with the CoFeB/MgO system at reduced dimensions less than 20 nm [9,10].

First-principles calculations indicated that the interfacial perpendicular anisotropy is brought about by the hybridization of Fe $3d$ and O $2p$ orbitals [11]. The calculation is supported by an experimental work on x-ray magnetic circular dichroism, which showed that the anisotropy is related to Fe $3d$ orbital anisotropy at the CoFeB/MgO interface [12]. While the origin of the interfacial anisotropy appears to be well understood, the origin of its temperature dependence, which is important for further development of p-MTJs, is still to be elucidated.

As shown by Callen and Callen, the temperature T dependence of the anisotropy energy density K of ferromagnets has a correlation with that of the spontaneous magnetization M_S through a power-law scaling relationship [13],

$$\frac{K(T)}{K(T^*)} = \left(\frac{M_S(T)}{M_S(T^*)}\right)^n, \tag{1}$$

where T^* is a normalizing temperature originally taken as 0 K. In this study we choose 10 K as T^*, the lowest measurement temperature, at which thermal spin fluctuation is expected to be small. The exponent n is known to depend on the physical mechanism causing the magnetic anisotropy; n is equal to 3 for materials with a uniaxial single-ion anisotropy [13], and is closer to 2 for materials with a dominant two-site anisotropy [14]. However, one may need to care about a mixture of the effects from bulk and surface properties on the anisotropy in thin films and nanoparticles with interfacial anisotropy [15]. Hence, the investigation of the correlation between K and M_S

*hsato@riec.tohoku.ac.jp
†richard.evans@york.ac.uk

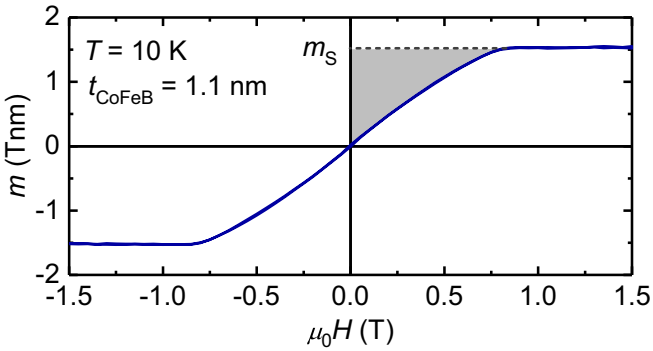

FIG. 1. Magnetic moment m per unit area versus in-plane magnetic field H for 1.1-nm-thick CoFeB film measured at 10 K. From the shaded area, areal magnetic anisotropy energy density $K_{eff}t_{CoFeB}$ is evaluated.

as a function of T is expected to provide us an insight of the exchange mechanism relating to the interfacial anisotropy.

In this study, we investigate the temperature dependence of M_S and K of the thin CoFeB/MgO system. We compare the experimental results with atomistic spin-model simulations [16], and show that their temperature dependence is related to thermal spin fluctuations and the finite thickness of the system.

II. EXPERIMENT

A. Film fabrication and measurement method

A stack structure of Ta (5)/Ru (10)/Ta (5)/$Co_{20}Fe_{60}B_{20}$ (t_{CoFeB})/MgO (1.4)/Ta (5) was deposited on a thermally oxidized Si substrate by rf magnetron sputtering. Numbers in parentheses are nominal thicknesses in nm determined from the deposition rate. We prepared five samples with different CoFeB thicknesses (t_{CoFeB} = 1.1, 1.3, 1.7, 3.0, and 4.0 nm). The CoFeB composition is also nominal, and corresponds to that of a sputtering target. The boron composition of the film is probably higher than the nominal one, while the composition ratio of Co to Fe is almost the same [17]. The stacks were annealed in vacuum at 300 °C for 1 h under an out-of-plane magnetic field of 0.4 T. We do not expect the formation of a magnetically dead layer in the structures as shown in the previous work [8]. We measured the magnetization curve for the stacks along the hard-axis direction at various temperatures by a vibrating sample magnetometer. A typical magnetization curve is shown in Fig. 1 for the stack with t_{CoFeB} = 1.1 nm at 10 K. From the curves, we determined the spontaneous magnetic moment per unit area m_S and areal effective perpendicular magnetic anisotropy energy density $K_{eff}t_{CoFeB}$ (the area enclosed by the m-H curve and $m = m_S$ in Fig. 1) [8].

B. Results

Figure 2(a) shows the temperature dependence of M_S between 10 and 300 K as a function of t_{CoFeB}, where M_S was determined from $M_S = m_S/t_{CoFeB}$. The M_S exhibits a monotonic decreasing tendency in all the CoFeB films with different t_{CoFeB} within experimental errors. The thinner CoFeB film ($t_{CoFeB} < 2$ nm) shows a larger variation of M_S with increasing temperature, as noticed from Fig. 2(b), in which

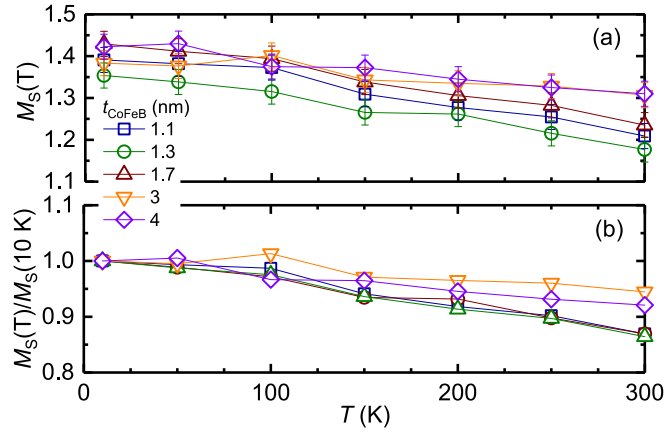

FIG. 2. Temperature T dependence of (a) spontaneous magnetization M_S and (b) normalized $M_S(T)/M_S(10\ K)$ for CoFeB/MgO stacks as a function of CoFeB thicknesses t_{CoFeB}.

the normalized spontaneous magnetization $M_S(T)/M_S(10\ K)$ is presented.

Figure 3(a) shows the temperature dependence of the perpendicular anisotropy energy density $K = K_{eff} + {M_S}^2/2\mu_0$, where μ_0 is permeability in free space, as a function of t_{CoFeB}. Because the interfacial anisotropy plays a dominant role for the perpendicular anisotropy in the CoFeB/MgO system, K is approximately equal to K_i/t_{CoFeB}, where K_i is the interfacial anisotropy energy density. As can be seen, K decreases with increasing T, indicating that K_i also decreases with increasing T. The thinner CoFeB film ($t_{CoFeB} < 2$ nm) shows a larger variation of K with change in T, as noticed from Fig. 3(b), in which the normalized anisotropy energy density $K(T)/K(10\ K)$ is presented.

Figure 4 shows the double-logarithm plot of $K(T)/K(10\ K)$ versus $M_S(T)/M_S(10\ K)$ as a function of t_{CoFeB}. A linear fit to the data for the samples with $t_{CoFeB} < 2$ nm gives the slope n of 2.2, in agreement with previous experimental measurements [18–20]. The scaling exponent $n \sim 2$ suggests that the anisotropy is not dominated by single-ion anisotropy with

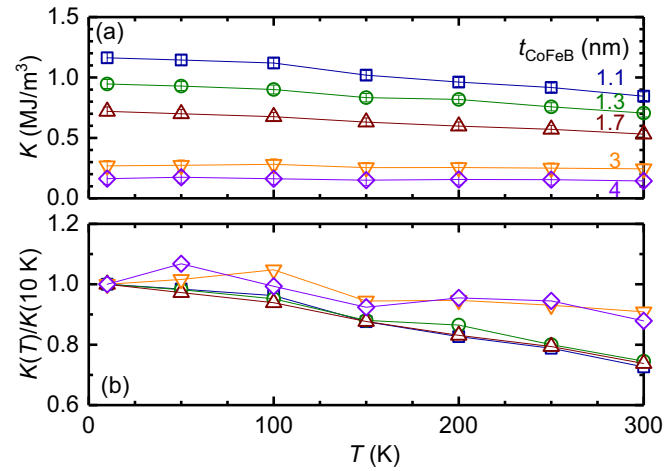

FIG. 3. Temperature T dependence of (a) perpendicular anisotropy energy density K and (b) normalized $K(T)/K(10\ K)$ for CoFeB/MgO stacks as a function of CoFeB thicknesses t_{CoFeB}.

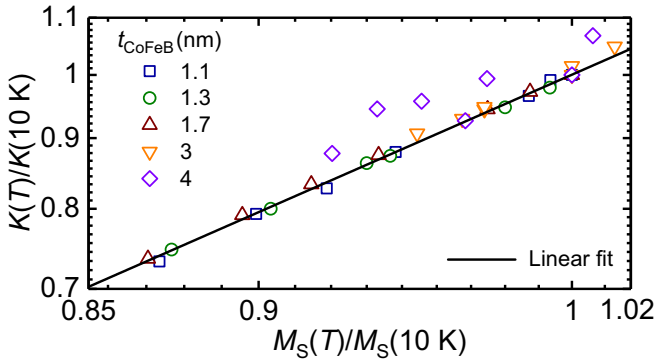

FIG. 4. Double-logarithm plot of $K(T)/K(10\ \mathrm{K})$ versus $M_S(T)/M_S(10\ \mathrm{K})$ for CoFeB/MgO with different CoFeB thicknesses t_{CoFeB}. Line is a linear fit for the sample with $t_{CoFeB} < 2$ nm.

$n = 3$ according to the Callen-Callen theory [13]. A similar experimental scaling exponent of $n \sim 2.1$ was observed for FePt [21], and was explained theoretically by a model based on two-site exchange anisotropy [14].

III. SIMULATIONS

A. Atomistic spin model with single-ion anisotropy

The simulations are based on the atomistic spin model [22], which naturally models the influence of thermal spin fluctuations on the intrinsic magnetic properties such as the spontaneous magnetization and magnetic anisotropy. We use a classical atomistic spin model utilizing the VAMPIRE software package for the numerical calculations [22,23]. The spin Hamiltonian using the Heisenberg form of exchange,

$$\mathscr{H} = -\sum_{i<j} J_{ij}\mathbf{S}_i \cdot \mathbf{S}_j - \sum_i k_u(\mathbf{S}_i \cdot \mathbf{e}_i)^2, \qquad (2)$$

describes the energy of the system, where J_{ij} is an isotropic exchange constant between nearest-neighbor spins as usual in the Heisenberg model, $\mathbf{S}_i$ and $\mathbf{S}_j$ are spin unit vectors at local sites i and nearest-neighbor sites j, respectively, k_u is the uniaxial anisotropy constant per atom, and $\mathbf{e}_i$ is a unit vector along the magnetic easy axis.

The simulated system is shown schematically in Fig. 5. The system is generated by creating a bulk body-centered-

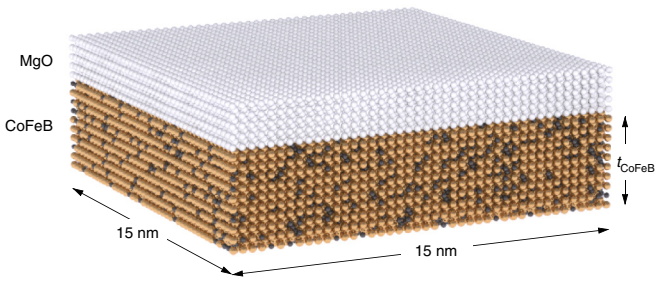

FIG. 5. Schematic of the simulated system incorporating bulk and interfacial CoFeB in contact with the MgO layer. The system dimensions are 15 nm × 15 nm × t_{CoFeB} nm, where t_{CoFeB} is the thickness of the CoFeB layer. Boron impurities indicated by dark spheres are randomly distributed through the CoFeB.

TABLE I. Adopted model parameters.

	Bulk	Interface
k_u (J/atom)	0	1.35×10^{-22}
J_{ij} (J/link)	7.735×10^{-21}	1.547×10^{-20}

cubic (bcc) crystal with lattice constant of 0.286 nm. The dimensions of CoFeB layer in the simulation are 15 nm × 15 nm × t_{CoFeB} nm, with periodic boundary conditions in the in-plane x and y directions. The Fe and Co atoms are treated as an average species with an averaged moment of $1.6\mu_B$ (μ_B is the Bohr magneton). This approximation is not expected to strongly affect the calculated temperature dependence of M_S and K resulting from the thermal spin fluctuations. The boron atoms are included explicitly as nonmagnetic impurities randomly distributed in the CoFeB. Despite the boron being nonmagnetic, it strongly affects the magnetic properties, because the presence of the impurities reduces the number of coordination of the magnetic atoms, and thus reduces the effective Curie temperature of the whole sample. As with boron, the MgO is nonmagnetic, but has a strong influence on the magnetic properties of the interfacial Co and Fe atoms. We consider two important effects: one is the presence of strong interfacial anisotropy k_u [24], and the other is an enhancement of the exchange interaction J_{ij} at the CoFeB/MgO interface [25]. We model the interfacial anisotropy using an effective uniaxial anisotropy for the CoFeB/MgO interfacial layer guided by previous first-principles calculations showing a localized enhancement of the anisotropy at the CoFeB/MgO interface [11]. The enhancement of the interfacial exchange interaction is treated in the same nearest-neighbor approximation as the bulk CoFeB but with an enhanced exchange constant. The adopted values of k_u and J_{ij} are listed in Table I. The k_u is derived from the experimental results in Fig. 3, and the exchange constant J_{ij} is derived from a mean-field expression of the effective exchange energy [22] including a correction for spin-wave excitations [26]. The bottom interfacial layer of CoFeB to be in contact with Ta is assumed to have no special interfacial qualities other than the usual loss of coordination. We do not consider the bulk anisotropy of the CoFeB, as experimentally it is known to be negligibly small [8].

The temperature-dependent properties are calculated using the constrained Monte Carlo method [16], in which the direction of the magnetization is fixed, while the net magnetization can be changed due to thermal fluctuations. The computational approach chooses moves of two spins, which are rotated in such a way as to conserve the direction of the magnetization. The static properties can be calculated when the system achieves thermal equilibrium after many such moves. Due to the symmetry of the system (consisting of a single high-anisotropy interface layer with periodic boundaries in the plane), the interfacial anisotropy is wholly uniaxial in nature, resulting in the angle-dependent torque following a $\sin\theta$ form at all temperatures, where θ is the angle from the film normal. Applying a quadrature rule, the effective anisotropic free energy is calculated directly from the thermodynamic average of the total torque on the system [16]. Given the $\sin\theta$ form of the torque, we fix θ at 45°, at which the

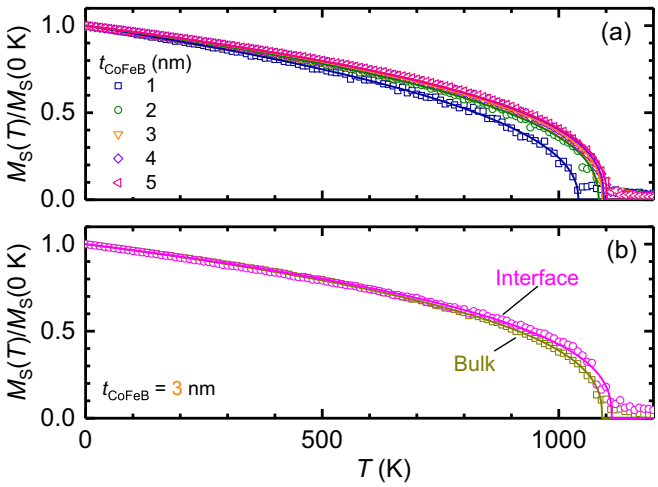

FIG. 6. Simulated temperature T dependence of normalized spontaneous magnetization $M_S(T)/M_S(0)$ for the CoFeB/MgO system with B composition of 4% (a) as a function of CoFeB thicknesses t_{CoFeB} and (b) surface and bulk components for CoFeB with $t_{CoFeB} =$ 3 nm. Lines are fits by Eq. (3).

torque is largest, to minimize the numerical error. The Monte Carlo (MC) trial moves use the Hinzke-Nowak method using a combination of different trial moves to optimize the relaxation to thermal equilibrium [27]. After equilibrating the system by 10 000 MC steps, the thermodynamic averages of the torque and magnetization are collected averaging over further 10 000 MC steps.

B. Calculation of the spontaneous magnetization

Because of $J_{ij} \gg k_u$, the anisotropy has a negligible effect on the calculated $M_S(T)$. Figure 6(a) shows the calculated $M_S(T)$ normalized by $M_S(T = 0)$ as a function of t_{CoFeB} of the CoFeB/MgO system with B composition of 4%. The value of 4% is extracted from a series of calculations to give the best agreement with the experimentally measured temperature-dependent magnetization. The reduced boron composition in the simulation is consistent with an experimental result that the boron composition in the CoFeB film is reduced owing to absorption by Ta adjacent to the CoFeB layer via annealing [28].

Because the CoFeB layers consist of a few monolayers, the magnetization curves in Fig. 6(a) show significant finite-size effects. This is apparent in the reduced criticality of the magnetization curve compared with a bulk sample, as well as a visible variation among samples with different t_{CoFeB}. It is clear from the simulations that the low-temperature gradient of the magnetization is thickness dependent, as seen also in the experimental data (Fig. 2). Quantitative agreement between the experimental data and simulations is obtained for thin CoFeB after tuning the boron concentration in the simulations.

Both experimental and simulated sets of data show a decrease in the gradient with increasing t_{CoFeB}. In the case of the simulations, this decrease is purely due to finite-size effects. As the film thickness increases, the thermally fluctuating surface spins make up a smaller portion of the total magnetization, and thus the gradient approaches the classical limit for the bulk with a slower variation of $M_S(T)$. For the experimental result, we see a similar behavior; however, the large change of the gradient for the thicker films seen in Fig. 2 may suggest the presence of an additional effect. For bulk CoFe, one would expect the usual Bloch-like behavior, where the gradient of the temperature-dependent magnetization is small due to the quantum nature of the spin-wave spectrum [29]. For the thin-film samples studied in the present work, however, it is clear that the gradient is much closer to that of a classical system, where the atomic spins are unquantized. We attribute this fundamental disparity to microstructural disorder and the polycrystalline nature of the films, which disrupt the long-range crystallinity and quantum nature of the spin waves. One would therefore expect that these effects become less important for larger film thicknesses, and so the larger decrease in the gradient of $M_S(T)$ compared to the classical simulations is indicative of a classical-quantum transition. This transition indicates an important finite-size effect, where the microstructural disorder can disrupt the quantum nature of the spin-wave spectrum leading to significantly different $M_S(T)$ from the expected bulk behavior.

The temperature-dependent magnetization $M_S(T)$ for a classical system is well described by the expression [29]

$$\frac{M_S(T)}{M_S(0)} = \left(1 - \frac{T}{T_C}\right)^{\beta}, \tag{3}$$

where β is a critical exponent. We fit Eq. (3) to simulated $M_S(T)$ treating T_C and β as free parameters. The obtained T_C is ~1100 K, which is not strongly dependent on t_{CoFeB}. However, it is important to note that the finite-size effect is visible in the larger magnetization fluctuations in the interface layers, which has a strong influence on the temperature dependence of the anisotropy. This is an important generic feature of ultrathin films, arising from the loss of magnetic coordination at the interface. In the case of CoFeB/MgO, an enhanced exchange interaction at the surface included in the simulation might be expected to somewhat compensate this effect [23].

To investigate the difference in the temperature dependence between interface and bulk-like magnetization, we have calculated separate contributions from the MgO-terminated interface and bulk atoms to the total magnetization, as shown in Fig. 6(b). The bulk atoms make up the majority of the complete system, and so the average magnetization is generally closer to the net magnetization. The temperature-dependent magnetizations show a slightly elevated Curie temperature for the MgO-terminated interface atoms compared with the bulk, owing to the stronger exchange interactions at the interface. The calculated Curie temperature for the interfacial atoms also converges rapidly to an asymptotic value. The temperature dependence of the interface magnetization is an important quantity that determines the spin fluctuations of the interfacial layer, which provides the magnetic anisotropy.

C. Calculation of the perpendicular anisotropy based on single-ion anisotropy

The magnetocrystalline anisotropy in the CoFeB/MgO system arises almost solely from the MgO-terminated interface. We proceed with calculation of the temperature dependence

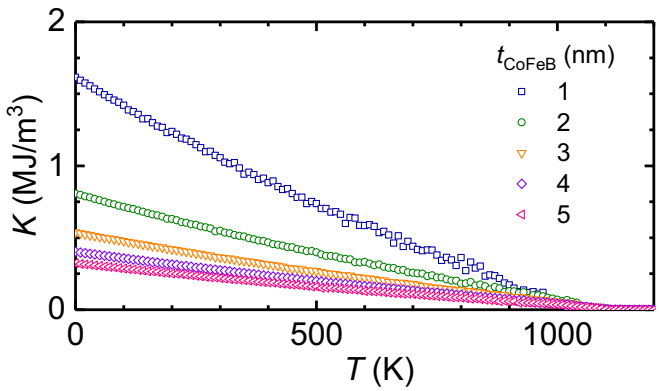

FIG. 7. Calculated temperature T dependence of magnetic anisotropy energy densities K for the CoFeB/MgO as a function of CoFeB thicknesses t_{CoFeB} based on single-ion anisotropy.

of the interface anisotropy using the constrained Monte Carlo method [16]. The calculated free anisotropy energy for different t_{CoFeB} is shown in Fig. 7(a). All samples have a single MgO-terminated interface with the same anisotropy energy, which leads to a change in the average magnetic anisotropy energy density, allowing engineering of the magnetic properties through thickness variation [8]. Additionally, the different temperature dependence of the surface magnetization leads to a different temperature dependence of the anisotropy for the samples with different t_{CoFeB}. According to Eq. (1), we make double-logarithm plots of $K(T)/K(10\ \mathrm{K})$ versus $M_{\mathrm{S}}(T)/M_{\mathrm{S}}(10\ \mathrm{K})$ (Callen-Callen plots) (as shown by dashed line in Fig. 9 shown later) [13]. We determine the scaling exponent n to be 2.82–3.26, which is close to 3 expected from single-ion anisotropy but inconsistent with the experimental observation in Fig. 4. This indicates that the magnetic anisotropy in CoFeB/MgO thin films is not single ion in origin.

D. Calculation of the perpendicular anisotropy based on two-site anisotropy

Two-site anisotropy arises from an orientation-dependent exchange interaction. For example, in layered $L1_0$ alloys such as FePt, the symmetry of the crystal along the c axis causes an asymmetry in the exchange interactions between atoms in the same plane [14,15] leading to a two-site exchange anisotropy. This is also expected to be the case for CoFeB/MgO layers, where the hybridization of the interfacial Fe layer leads to a change in symmetry along the z direction. The two-site anisotropy can be expressed by an exchange tensor as a perturbation of the usual isotropic exchange,

$$J_{ij}^{\mathrm{T}} = \begin{bmatrix} J_{xx} & 0 & 0 \\ 0 & J_{yy} & 0 \\ 0 & 0 & J_{zz} \end{bmatrix}, \tag{4}$$

where subscripts to J of tensor components denote the components of the spin direction at i and j sites. For a system with only two-site anisotropy, the spin Hamiltonian is given by

$$\mathscr{H}_{\mathrm{ex}} = -\sum_{i<j} \mathbf{S}_i J_{ij}^{\mathrm{T}} \mathbf{S}_j. \tag{5}$$

In the case of isotropic exchange, all the diagonal exchange components are the same, $J_{xx} = J_{yy} = J_{zz}$. For anisotropic exchange with asymmetry along the z direction, $J_{xx} = J_{yy} \neq J_{zz}$.

The value of the effective anisotropy at very low temperatures is the same and independent of its physical origin, where the origin is only evident from the scaling with respect to the magnetization. Therefore, in our model we must translate the value of anisotropy from Sec. II C into a two-site exchange anisotropy. Considering the exchange interactions between two spins S_i and S_j, we have the total exchange energy $E_{\mathrm{ex}} = -J_{xx}S_{ix}S_{jx} - J_{yy}S_{iy}S_{jy} - J_{zz}S_{iz}S_{jz}$, where subscripts for $S_{i(j)}$ denote the x, y, and z components of spin at $i(j)$ site, respectively. In ferromagnets at low temperatures, all spins are well aligned and so it can be assumed that $\mathbf{S}_i \approx \mathbf{S}_j$. For the case with an easy axis along the z direction and spin rotation in the z-x plane ($S_z = \cos\theta$ and $S_x = \sin\theta$), we obtain $E_{\mathrm{ex}} = (J_{zz} - J_{xx})\sin^2\theta - J_{zz}$, and thus the anisotropic exchange gives the exchange energy with an identical $\sin^2\theta$ symmetry to the single-ion anisotropy. The total two-site exchange anisotropy is expressed by the difference in the diagonal values of the exchange tensor $J_{zz} - J_{xx}$. For spins with several neighbors, the anisotropy energy should be divided amongst each of the interactions to give the same effective anisotropy. In the case of a nearest-neighbor model the coordination number defines the number of interactions, giving geometric factors of $1/6$ for simple cubic, $1/8$ for bcc, and $1/12$ for face-centered-cubic and hexagonal lattices. The CoFeB/MgO interfacial anisotropy is a special case, since the anisotropy arises from the Fe-O hybridization and the interfacial atoms are only half coordinated. In this case, the anisotropic exchange energy should be divided among the four nearest atoms in the interface, giving a geometric factor of $1/4$. In this case, the exchange values at the interface in terms of the parameters from Table I are given by

$$J_{xx} = J_{ij}, \quad J_{yy} = J_{ij}, \quad J_{zz} = J_{ij} + k_{\mathrm{u}}/4. \tag{6}$$

The bulk parameters are unchanged. Revisiting the simulations using the spin Hamiltonian given in Eq. (5), we now explicitly exclude any single-ion contribution to the effective

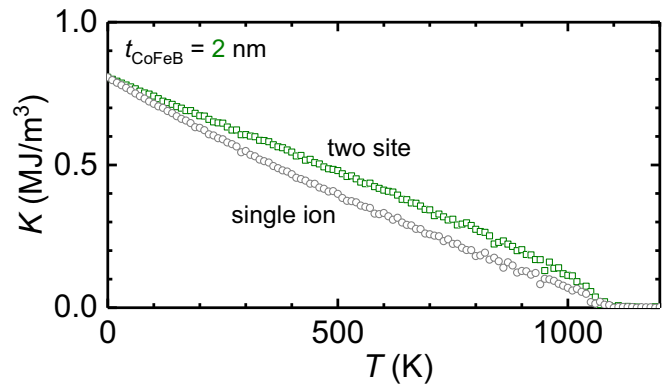

FIG. 8. Calculated temperature T dependence of magnetic anisotropy energy densities K for the CoFeB/MgO with 2-nm-thick CoFeB based on two-site anisotropy along with that based on single-ion anisotropy shown in Fig. 7.

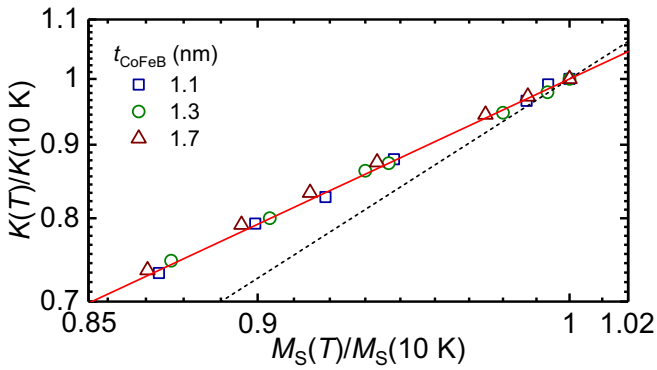

FIG. 9. Double-logarithm plot of $K(T)/K(10\ \mathrm{K})$ versus $M_S(T)/M_S(10\ \mathrm{K})$ for CoFeB/MgO. Symbols correspond to the experimental results for the samples with CoFeB thicknesses less than 2 nm. Lines are determined from linear fitting to the simulated results (solid line for two-site anisotropy and dashed line for single-ion anisotropy).

anisotropy. We note that in both cases the total effective interfacial anisotropy at zero temperature is the same. The obtained $K(T)$ is shown in Fig. 8.

The scaling plots between $K(T)/K(10\ \mathrm{K})$ and $M_S(T)/M_S(10\ \mathrm{K})$ give the scaling exponent n of 2.21, which is consistent with the experimental observation as shown in Fig. 9. The result indicates that the Callen-Callen plot gives $n \sim 2$ for systems with two-site anisotropy [14], indicating that the Callen-Callen plot can be used to gain insight into the origin of the anisotropy [30].

IV. CONCLUSION

We have conducted a joint experimental and computational study on the temperature-dependent magnetization and magnetic anisotropy of CoFeB/MgO ultrathin films. Our experimental measurements have found the strong temperature dependence of the saturation magnetization in close agreement with classical atomistic spin-model simulations. The scaling of the anisotropy with the magnetization provides direct insight into the physical origin of the anisotropy by comparison with the Callen-Callen theory. From the Callen-Callen theory, a scaling exponent of $n = 3$ suggests local single-site anisotropy while an exponent of $n \sim 2$ suggests two-site exchange anisotropy. Experimental measurements give the scaling exponent of $n = 2.2$, indicating the dominant role of two-site exchange anisotropy in this material system. We have also performed atomistic simulations to compare with experimental observation by considering thermal fluctuations due to the finite-size effect and a reduction in atomic coordination at the interface. The atomistic simulations with single-ion anisotropy model result in $n = 3.03$ as expected, which does not agree with the experimental results. The simulations with purely two-site exchange anisotropy reproduce the experimentally observed value ($n = 2.2$). In this work, we assume identical magnetic atoms in a uniform structure and negligible anisotropy at CoFeB/Ta interface, suggesting that the temperature-dependent magnetic properties are determined mainly by the MgO/CoFeB interface. This study provides information of the important factors determining the temperature-dependent thermal stability of CoFeB/MgO magnetic tunnel junctions and to guide the design of structures for various applications.

ACKNOWLEDGMENTS

The work was partly supported by JSPS Core-to-Core Program and RIEC Cooperative Research Projects. The work at Tohoku University was supported by ImPACT program of CSTI and a Grant-in-Aid for Scientific Research from MEXT (Grant No. 26103002). This work made use of the facilities of N8 HPC Centre of Excellence, provided and funded by the N8 consortium and EPSRC (Grant No. EP/K000225/1), coordinated by the Universities of Leeds and Manchester. P.C. gratefully acknowledges the funding from Mahasarakham University.

[1] M. Klaua, D. Ullmann, J. Barthel, W. Wulfhekel, J. Kirschner, R. Urban, T. L. Monchesky, A. Enders, J. F. Cochran, and B. Heinrich, Phys. Rev. B **64**, 134411 (2001).

[2] S. Monso, B. Rodmacq, S. Auffret, G. Casali, F. Fettar, B. Gilles, B. Dieny, and P. Boyer, Appl. Phys. Lett. **80**, 4157 (2002).

[3] A. Manchon, C. Ducruet, L. Lombard, S. Auffret, B. Rodmacq, B. Dieny, S. Pizzini, J. Vogel, V. Uhlir, M. Hochstrasser, and G. Panaccione, J. Appl. Phys. **104**, 043914 (2008).

[4] L. E. Nistor, B. Rodmacq, S. Auffret, and B. Dieny, Appl. Phys. Lett. **94**, 012512 (2009).

[5] J. Hayakawa, S. Ikeda, F. Matsukura, H. Takahashi, and H. Ohno, Jpn. J. Appl. Phys. **44**, L587 (2005).

[6] D. D. Djayaprawira, K. Tsunekawa, M. Nagai, H. Maehara, S. Yamagata, N. Watanabe, S. Yuasa, Y. Suzuki, and K. Ando, Appl. Phys. Lett. **86**, 092502 (2005).

[7] M. Endo, S. Kanai, S. Ikeda, F. Matsukura, and H. Ohno, Appl. Phys. Lett. **96**, 212503 (2010).

[8] S. Ikeda, K. Miura, H. Yamamoto, K. Mizunuma, H. D. Gan, M. Endo, S. Kanai, J. Hayakawa, F. Matsukura, and H. Ohno, Nat. Mater. **9**, 721 (2010).

[9] H. Sato, E. C. I. Enobio, Y. Yamanouchi, S. Ikeda, S. Fukami, F. Matsukura, and H. Ohno, Appl. Phys. Lett. **105**, 062403 (2014).

[10] J. Z. Sun, S. L. Brown, W. Chen, E. A. Delenia, M. C. Gaidis, J. Harms, G. Hu, X. Jiang, R. Kilaru, W. Kula, G. Lauer, L. Q. Liu, S. Murthy, J. Nowak, E. J. O'Sullivan, S. S. P. Parkin, R. P. Robertazzi, P. M. Rice, G. Sandhu, T. Topuria, and D. C. Worledge, Phys. Rev. B **88**, 104426 (2013).

[11] R. Shimabukuro, K. Nakamura, T. Akiyama, and T. Ito, Physica E **42**, 1014 (2010).

[12] S. Kanai, M. Tsujikawa, Y. Miura, M. Shirai, F. Matsukura, and H. Ohno, Appl. Phys. Lett. **105**, 222409 (2014).

[13] H. Callen and E. Callen, J. Phys. Chem. Solids **27**, 1271 (1966).

[14] O. N. Mryasov, U. Nowak, K. Y. Guslienko, and R. W. Chantrell, Europhys. Lett. **69**, 805 (2005).

[15] R. Yanes, O. Chubykalo-Fesenko, R. F. L. Evans, and R. W. Chantrell, J. Phys. D: Appl. Phys. **43**, 474009 (2010).

[16] P. Asselin, R. F. L. Evans, J. Barker, R. W. Chantrell, R. Yanes, O. Chubykalo-Fesenko, D. Hinzke, and U. Nowak, Phys. Rev. B **82**, 054415 (2010).

[17] H. D. Gan, S. Ikeda, M. Yamanouchi, K. Miura, K. Mizunuma, J. Hayakawa, F. Matsukura, and H. Ohno, IEEE Trans. Magn. **47**, 1567 (2011).

[18] H. D. Gan, H. Sato, M. Yamanouchi, S. Ikeda, K. Miura, R. Koizumi, F. Matsukura, and H. Ohno, Appl. Phys. Lett. **99**, 252507 (2011).

[19] J. G. Alazate, P. K. Amiri, G. Yu, P. Upadhyaya, and J. A. Katine, Appl. Phys. Lett. **104**, 112410 (2014).

[20] A. Okada, S. He, B. Gu, S. Kanai, A. Soumyanarayanan, S. S. T. Lim, M. Tran, M. Mori, S. Maekawa, F. Matsukura, H. Ohno, and C. Panagopoulos, Proc. Natl. Acad. Sci. USA **114**, 3815 (2017).

[21] S. Okamoto, N. Kikuchi, O. Kitakami, T. Miyazaki, Y. Shimada, and K. Fukamichi, Phys. Rev. B **66**, 024413 (2002).

[22] R. F. L. Evans, W. J. Fan, P. Chureemart, T. A. Ostler, M. O. A. Ellis, and R. W. Chantrell, J. Phys.: Condens. Matter **26**, 103202 (2014).

[23] VAMPIRE software package, Version 4. Available from http://vampire.york.ac.uk/.

[24] H. X. Yang, M. Chshiev, B. Dieny, J. H. Lee, A. Manchon, and K. H. Shin, Phys. Rev. B **84**, 054401 (2011).

[25] I. Turek, S. Blugel, G. Bihlmayer, and P. Weinberger, Czech. J. Phys. **53**, 81 (2003).

[26] D. A. Garanin, Phys. Rev. B **53**, 11593 (1996).

[27] D. Hinzke and U. Nowak, Comput. Phys. Commun. **121**, 334 (1999).

[28] S. V. Karthik, Y. K. Takahashi, T. Ohkubo, K. Hono, H. D. Gan, S. Ikeda, and H. Ohno, J. Appl. Phys. **111**, 083922 (2012).

[29] R. F. L. Evans, U. Atxitia, and R. W. Chantrell, Phys. Rev. B **91**, 144425 (2015).

[30] R. Skomski, O. N. Mryasov, J. Zhou, and D. J. Sellmyer, J. Appl. Phys. **99**, 08E916 (2006).